conference papers

Surface free energies of isotactic polybutene-1 tetragonal and trigonal crystals: the role of conformational entropy of side chains

Motoi Yamashita* and Minoru Kato

Department of Applied Chemistry, Ritsumeikan University, 1-1-1 Noji-higashi, Kusatsu, Shiga 525-8577, Japan.
Correspondence e-mail: motoi-y@is.ritsumei.ac.jp

Lateral and end surface free energies of melt-crystallized isotactic polybutene-1 (it-PB1) trigonal and tetragonal crystals have been determined by small-angle X-ray scattering and *in situ* observation of the crystal growth kinetics. The lateral surface free energy σ of the trigonal phase is about seven times as large as the value σ^{Hoff} calculated according to Hoffman's equation [Hoffman (1992). *Polymer*, **33**, 2643–2644], while that of the tetragonal phase is roughly in agreement with the estimation. The discrepancy between the values of σ and σ^{Hoff} for the trigonal phase can be attributed to the loss of conformational entropy of the ethyl side chains of it-PB1.

1. Introduction

Surface free energies of crystals are of critical importance in the understanding of crystal growth mechanisms. They contribute to the barrier of surface nucleating processes and are the main factor determining the crystal growth kinetics. In the standard theory of crystal growth of polymers, surface free energy of two lateral surfaces of a surface nucleus is interpreted as the free energy barrier to form a surface nucleus.

The origin of crystal surface free energy has been studied extensively. In monatomic systems, Spaepen (1975) proposed that surface free energy should be basically of entropic origin, not of energetic origin. Spaepen showed that surface free energy originates from the loss of configurational entropy when liquid adjusts itself to a crystal surface in order to minimize its interfacial density and energy deficit; liquid atoms at the crystal–liquid interface can not sample as many configurations as in the bulk because of the special boundary conditions of the crystal plane. This concept was introduced into the systems of *n*-alkanes as a 'negentropic model' by Turnbull & Spaepen (1978). In this case, the adjustment consists of orienting the molecular segments of the melt near the interface so that they are parallel to the crystal boundary plane. In 1992, Hoffman related the segmentallization of chain molecules to the characteristic ratio C_∞ of a rotational isometric state model of the melt state of polymers, and succeeded to express the lateral surface free energy σ of polymer crystals grown in the melt in a unified manner as follows:

$$\sigma = T\left(\frac{\Delta h_{\mathrm{f}}}{T_{\mathrm{m}}^0}\right)\left(\frac{a}{2}\right)\left(\frac{l_{\mathrm{b}}}{l_{\mathrm{u}}}\right)\frac{1}{C_\infty} \equiv \sigma^{\mathrm{Hoff}}, \tag{1}$$

where Δh_{f} is the heat of fusion per unit volume of crystal, T_{m}^0 the equilibrium melting temperature, a the width of the stem, l_{b} the bond length and l_{u} the C—C distance as projected along the c axis. The conventional nucleation theory explains that the free energy barrier of nucleation is the barrier to build two lateral surfaces of a surface nucleating stem. In the derivation of equation (1), Hoffman assumed that the barrier of nucleation results from the reduction of conformational entropy for polymer chains to become 'segmentalized' into sections of persistence length $C_\infty l_{\mathrm{b}}$ and 'aligned' along the growth

front before they become crystallographically attached into the crystal phase; this shows up as the lateral surface free energy. This depiction means that the lateral surface free energy originates from the loss of conformational entropy for polymer chains to be 'segmentalized and aligned', *i.e.* stretched along the growth face. The derivation of equation (1) is given in the Appendix.

Equation (1) has been successful in predicting the values of σ for a number of melt-crystallized polymers with simple side chains such as polyethylene (PE), isotactic polypropylene (it-PP), and poly(L-lactic acid) (Hoffman, 1992). This equation, however, does not hold for polymers with larger side chains such as isotactic polystyrene (it-PS) (Hoffman & Miller, 1997).

To elucidate the reason why equation (1) does not hold for polymers with larger side chains on the basis of experimental data, we determined the lateral surface free energies of isotactic polybutene-1 (it-PB1) tetragonal and trigonal crystals grown in the melt from small-angle X-ray scattering (SAXS) experiments and crystal growth kinetics observations. it-PB1 is a semicrystalline polyolefin and has ethyl groups as the side chains. it-PB1 exhibits stable trigonal form with 3/1 helical chains and metastable tetragonal form with 11/3 helical chains as the most common structures, as shown in Table 1. Crystallization in the bulk melt under atmospheric pressure yields the tetragonal form (Turner-Jones, 1963). The trigonal form is usually obtained from the solid–solid spontaneous transformation from the tetragonal form (Natta *et al.*, 1960) and in solutions (Holland & Miller, 1964). The trigonal form was recently shown to crystallize directly from the melt under atmospheric pressure with the aid of epitaxy (Kopp *et al.*, 1994) or in ultrathin films at an elevated temperature (Zhang *et al.*, 2002). In these works, however, *in situ* observations of the trigonal crystal growth could not be performed. In our previous work, we developed another method to crystallize the trigonal phase in the melt *via* self-seeding using solution grown trigonal crystals as nuclei and performed *in situ* observations of its growth process (Yamashita *et al.*, 2004, 2007).

In this work, we determine the lateral and end surface free energies of the trigonal form from experiments. We also determine those of the tetragonal form obtained from the same molten environment. We find the σ value of the tetragonal form is roughly in agreement with

Table 1
Physical properties of it-PB1.

| | T_g† (K) | U‡ (J mol^{-1}) | l_{b} (Å) | Unit-cell parameters | | | | Stem parameters | | | | | |
				a_0 (Å)	b_0 (Å)	c_0 (Å)	ρ§ (g cm^{-3})	a (Å)	b (Å)	Δh_f¶ (J m^{-3})	Space group	l_u (Å)	Chain conformation (monomers/turn)
Trigonal††				17.7	17.7	6.5	0.96	5.1	8.85	1.35×10^8	$\bar{R}3c$	1.08	3/1
Tetragonal‡‡				14.6	14.6	21.2	0.888	7.3	7.3	1.09×10^8	$\bar{P}4b2$	0.964	11/3
Amorphous	219.0	6280	1.54				0.87						

† Andrews & Grulke (1999).   ‡ Hoffman *et al.* (1976).   § Miller (1999).   ¶ Leute & Dollhopf (1983).   †† Natta *et al.* (1960).   ‡‡ Tashiro *et al.* (1998).

the theoretical value σ^{Hoff} whereas the σ value of the trigonal form clearly deviates from σ^{Hoff}. We present an attempt to investigate the role of side chain conformation in surface nucleation processes by comparison of these σ values with their corresponding σ^{Hoff} values. We will discuss the mechanisms in which equation (1) does not hold for the trigonal form taking conformational entropy of the side chains into consideration.

2. Experimental

2.1. Lamellar crystal thickness

The it-PB1 used in this study was purchased from Scientific Polymer Products ($\overline{M}_w$ = 185000; the melt index is 20 g 10 min^{-1}).

We measured the density ρ of samples by float and sink method using mixed solvents of water and ethanol at 298 K; crystallinity φ was determined from the density using the following equation:

$$\rho = \rho_c \varphi + \rho_a (1 - \varphi), \qquad (2)$$

where ρ_c and ρ_a are the density of crystalline and amorphous phases, respectively, listed in Table 1.

SAXS photographs were taken with a SAXS camera (camera length 414 mm) in vacuum to obtain lamellar long spacings, using an imaging plate system (Rigaku R-AXIS DSII). Nickel-filtered Cu $K\alpha$ X-ray radiation was used, generated at 50 kV and 140 mA. After the subtraction of the background intensity, isotropic two-dimensional data were circularly averaged to obtain one-dimensional data and corrected for the Lorentz factor. Application of Bragg's law to the scattering maxima was used to calculate the first- and second-order long spacings, L_1 and L_2. The lamellar crystal thickness, l_c, was estimated using the equation: $l_c = \varphi L_1$.

We prepared tetragonal samples by melt crystallization; then, we aged the tetragonal samples for 10 d at room temperature and obtained trigonal samples by spontaneous tetragonal–trigonal solid state transformation. Films of it-PB1 of about 500 µm thickness were sandwiched between aluminium foil and melted at 423.2 K for 3 min in an oven, transferred quickly to a hot-stage (Mettler FP82) kept at crystallization temperatures of 313.2, 343.2, 353.2, 363.2 and 373.2 K. Crystals of semicrystalline polymers are often known to exhibit thermal thickening when they are heated. To obtain long spacings just before the melting of the two forms, we carried out annealing of tetragonal and trigonal samples. Tetragonal films (as-crystallized samples) and trigonal films (aged samples) were transferred to another hot stage (Linkam LK-FDCS II), heated to the melting points determined by the differential scanning calorimetry (DSC) measurements described below at a rate of 30 K min^{-1} and cooled to room temperature at a rate of 50 K min^{-1}. The annealed trigonal films were used for SAXS and density measurements of the trigonal phase. The annealed tetragonal films were aged at room temperature for 10 d and used as samples for SAXS and density measurements of the tetragonal phase. In 10 d of aging at room temperature the

annealed tetragonal crystals transform into the trigonal form without changing their stacked lamellae structure and overall mass degree of crystallinity just before melting. Since the crystal density of the trigonal form is larger than that of the tetragonal form, SAXS intensity is much enhanced after 10 d. We determined l_c of the annealed-aged samples, then calculated l_c of the as-annealed tetragonal samples from the observed values of l_c of the annealed-aged samples assuming that l_c(as-annealed) = l_c(annealed-aged)/1.12. This assumption is based on the fact that the tetragonal–trigonal transformation involves an extension of the 11/3 helical conformation (tetragonal form) into the 3/1 helix (trigonal form). The ratio between the axial repeating units of this conformation is 1.12.

2.2. Melting point temperature

DSC measurements (Rigaku DSC-10A) were performed at a heating rate of 30 K min^{-1}. The melting temperatures of trigonal and tetragonal crystals were determined from the onset temperature of the endothermic peak. Samples used for DSC were crystallized under the same conditions as those of samples for SAXS. it-PB1 films just after crystallization were used as samples of tetragonal crystals; it-PB1 films stored at room temperature for 10 d after crystallization were used as samples of trigonal crystals.

2.3. Growth rate

In situ observations of the crystallization process were carried out using an optical microscope (Nikon OPTIPHOT2) with a hot stage (Mettler FP82). For the experiments of the tetragonal form, films of it-PB1 at a thickness of about 50 µm were sandwiched between two cover glasses and melted at 413.2 K for 2 min and cooled to a crystallization temperature between 325.2 K and 385.1 K. The growth rate was determined from the time dependence of the radius of spherulites or the major axis of axialites. For the crystal growth of the trigonal form, cast films were used; thin it-PB1 films were prepared by casting a 0.1 wt% *p*-xylene solution onto a carbon-coated mica kept at 333.2 K on a hot plate. The films were dried in air, an appropriate film thickness of *ca* 80 nm being judged by a gold interference colour. The it-PB1 films were heated at 401.2–409.2 K for 2 min and cooled to a crystallization temperature between 338.2 K and 361 K at a rate of 15 K min^{-1}. The growth rate was determined from the time dependence of the radius or the major axis of crystals observed by optical microscopy.

2.4. Identification of crystal structure

Wide-angle X-ray scattering (WAXS) experiments were performed to identify the crystal structures. Nickel-filtered Cu $K\alpha$ radiation was used, generated at 35 kV and 40 mA. The system and procedure used for data acquisition and analysis were the same as those used for SAXS experiments. To identify crystal structures of cast film samples, transmission electron microscopy (TEM; Jeol JEM-
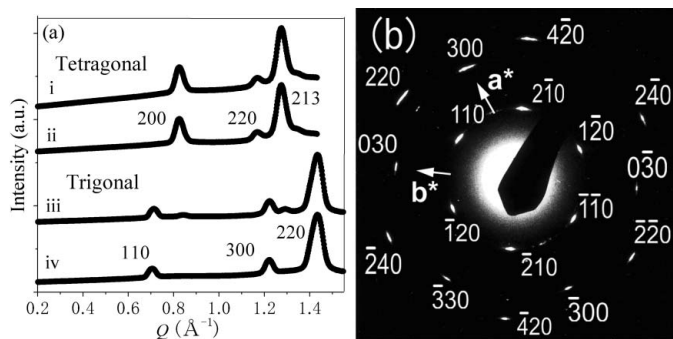
Figure 1
(a) WAXS profiles of it-PB1 tetragonal and trigonal crystals crystallized at 343.2 K before and just after annealing. Plots ii and iv represent data for samples after annealing. Peaks shown in plots i and ii are indexed with 200, 220, 213 reflections of the tetragonal form; peaks exhibited in plots iii and iv are indexed with 110, 300, 220 reflections of the trigonal form. ($Q = 4\pi\lambda^{-1}\sin\theta$, where θ is half the scattering angle and λ is the wavelength used.) (b) Electron diffraction pattern of an it-PB1 trigonal crystal grown in a molten cast film at 348.2 K showing hexagonal symmetry. Each of the diffraction spots could be indexed with the trigonal form of it-PB1.

1200EXII) was performed; samples immediately after crystallization and quench were examined. The it-PB1–carbon films were floated on a water surface and picked up on electron microscope grids and served as samples.

3. Results

3.1. Crystal structures from WAXS and TEM

We confirmed by WAXS measurements that samples immediately after the crystallization in the bulk melt, both as crystallized and as annealed, are in the tetragonal form (Fig. 1a). Hence, the observed growth rate and melting temperature of the samples crystallized in the bulk melt are those of tetragonal crystals; the observed crystallinity and lamellar crystal thickness obtained from annealed-aged samples reflect those of tetragonal crystals just before melting. Samples stored at room temperature for 10 d, both before and after annealing, exhibited peaks characteristic of the trigonal form (Fig. 1a). Therefore, the observed melting temperature of the samples stored after crystallization is that of the trigonal form; crystallinity and lamellar crystal thickness of annealed trigonal samples are those of the trigonal crystals just before melting. Crystals grown in molten cast films just after crystallization showed electron diffraction patterns of the trigonal phase (Fig. 1b); the growth rate of crystals observed in molten cast films is that of trigonal crystals.

3.2. Lamellar crystal thickness and melting temperature

Fig. 2 shows the Lorentz-corrected SAXS profiles for the tetragonal and trigonal samples. For both of the tetragonal and trigonal samples, first- and second-order reflections were observed in the wide range of crystallization temperatures from 313.2 to 363.2 K. Table 2 lists the DSC and SAXS results: crystallization and melting temperatures, the values of the first- and second-order long spacings, the ratios of the first-order long spacings to the second-order long spacings, degree of crystallinity and lamellar crystal thickness obtained from the tetragonal and trigonal samples.

The ratios of the first-order long spacings to the second-order long spacings are about two. For samples crystallized at 363.2 K, this ratio is 2.03 for the tetragonal and trigonal samples. At 373.2 K, only the second-order reflections were capable of being observed. By multiplying the second-order long spacings by the ratio at 363.2 K, 2.03, we

calculated the first-order long spacings of the tetragonal and trigonal samples at 373.2 K.

The melting temperature $T_m(l_c)$ of crystals with lamellar thickness l_c is expressed by the Gibbs–Thomson equation:

$$T_m(l_c) = T_m^0\left[1 - \frac{2\sigma_e}{\Delta h_f l_c}\right]. \qquad (3)$$

Fig. 3 shows the inverse of lamellar crystal thickness dependence of melting temperature for the trigonal and tetragonal forms. The data for both phases obey the linear relation given in equation (3), which gives the equilibrium melting point temperatures T_m^0 to be 409.3 K for the trigonal form and 397.2 K for the tetragonal form. The higher value of T_m^0 of the trigonal form than that of the tetragonal form plausibly corresponds to the higher values of T_m observed for the trigonal form than those observed for the tetragonal form. These T_m^0 values are slightly higher than the values 407.9 K for the trigonal form and 394.7 K for the tetragonal form obtained from dilatometry (Wilski & Grewer, 1964). The T_m^0 values in this work are in good agreement with the values 408.7 K for the trigonal form and 397.2 K for the tetragonal form determined by melting point depression (Danusso & Gianotti, 1963). The slope gives the value of $2\sigma_e T_m^0/\Delta h_f$ to be 2.48×10^3 Å K for the trigonal form and 3.17×10^3 Å K for the tetragonal form. The value of $\sigma_e/\Delta h_f$ is 3.03 Å for the trigonal form and 3.99 Å for the tetragonal form; σ_e is estimated as 4.11×10^{-2} J m^{-2} for the trigonal form and 4.36×10^{-2} J m^{-2} for the tetragonal form. Chain folding free energy $q = 2ab\sigma_e$ is calculated as 3.71×10^{-20} J stem^{-1} for the trigonal form and 4.65×10^{-20} J stem^{-1} for the tetragonal form by use of the stem parameters a and b in Table 1. The values of σ_e and q of the trigonal form are smaller than those of the tetragonal form. This is consistent with the fact that the trigonal form is more stable than the tetragonal form.

3.3. Growth rate

Both the trigonal and tetragonal crystals exhibited linear growth (figure not shown); the growth rate was found to be constant and was determined from the time derivative of the radius or major axis of crystals. Fig. 4 shows the logarithm of the growth rate G plotted against crystallization temperature for trigonal and tetragonal crystals. It is to be noted that the growth rate of trigonal crystals is one hundred times smaller than that of tetragonal crystals. In 1965, Powers et al. used trigonal crystals obtained by solid-state transformation from the tetragonal phase as nuclei and attempted to observe the growth of trigonal crystals in the melt. This was, unfortunately, not successful and they hypothesized that the growth rate of trigonal crystals is 'exceedingly' slower than that of tetragonal crystals. Our result is consistent with their prediction.

The nucleation theory by Hoffman & Miller (1997) describes the growth rate G observed at a crystallization temperature T by the following equation:

$$G = G_0 \exp\left[-\frac{U}{R(T - T_V)}\right]\exp\left[-\frac{K}{T\Delta T}\right], \qquad (4)$$

where G_0 and K are constants, U is the 'activation' energy for polymer diffusion, $R = kN_A$ (k is the Boltzmann constant and N_A is Avogadro's number), T_V is the Vogel temperature [$= T_g - 30$ (K); T_g is the glass transition temperature], ΔT ($= T_m^0 - T$) is a supercooling (T_m^0 is the equilibrium melting temperature). The first exponential factor is the Vogel–Fulcher factor for viscosity and the second exponential factor is the surface kinetic factor. Fig. 5 shows $\ln G + U/[R(T - T_V)]$ as a function of $1/(T\Delta T)$ for the two phases, using the parameters listed in Table 1 and the values of T_m^0 we determined

Table 2
Results of DSC, SAXS and crystallinity measurements of trigonal and tetragonal samples.

T_e = crystallization temperature, T_m = melting temperature, L_1 = the first-order long spacings, L_2 = the second-order long spacings, φ = crystallinity, l_c = lamellar crystal thickness. The l_c data for tetragonal samples are estimated values for as-annealed samples before aging; they were derived assuming l_c(as-annealed) = l_c(annealed-aged)/1.12. (See the text.)

T_e (K)	T_m (K)	L_1 (Å)	L_2 (Å)	L_1/L_2	φ (%)	l_c (Å)
Trigonal samples						
313.2	385.9	237	130	1.82	44.8	106
343.2	391.5	283	153	1.85	49.8	141
353.2	394.8	313	158	1.98	53.5	168
363.2	397.4	378	186	2.03	55.9	211
373.2	399.9	(459)	223	-	58.0	266
Tetragonal samples						
313.2	376.0	313	155	2.02	52.9	147
343.2	377.3	327	164	2.00	54.2	158
353.2	377.8	342	169	2.02	54.2	165
363.2	379.7	378	186	2.03	56.9	191
373.2	384.4	(452)	223	-	59.1	237

above. The value of $\ln G + U/[R(T-T_V)]$ depends on $1/(T\Delta T)$ linearly over the whole range examined for both phases. Equation (4) holds for all the crystallization temperature ranges investigated; the growth rate of it-PB1 trigonal and tetragonal crystals shows the temperature dependence derived from the nucleation theory.

The extrapolation to zero of the straight lines in Fig. 5 for $1/(T\Delta T)$ gives the values of G_0 to be 6.33×10^5 μm s^{-1} and 1.64×10^4 μm s^{-1} for trigonal and tetragonal crystals, respectively; the slopes give the values of K to be 2.73×10^5 K^2 for the trigonal form and 6.46×10^4 K^2 for the tetragonal form. The value of K obtained for the trigonal form is about 4.2 times as large as that obtained for the tetragonal form; this indicates that the kinetic barrier for crystallization of the trigonal form is 4.2 times larger than that of the tetragonal form. On the other hand, the value G_0 of the trigonal form is 39 times as large as that of the tetragonal form.

Assuming that the crystallization is in the regime of multiple nucleation on flat growth faces, regime II, K in equation (4) is represented by the following expression:
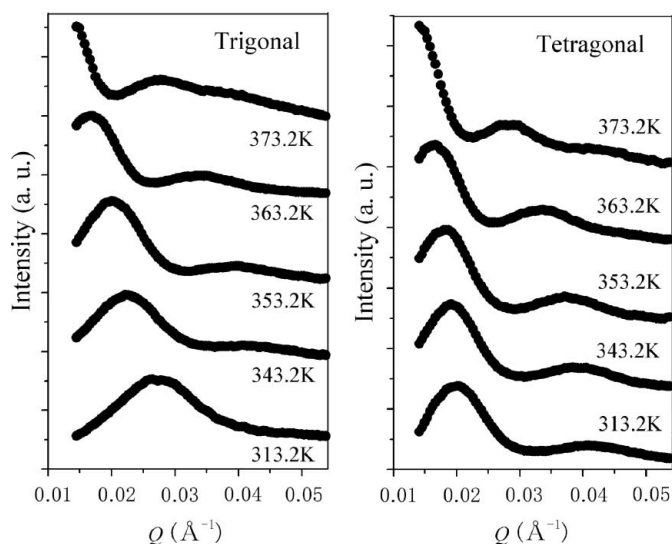
$$K = \frac{2b\sigma\sigma_e T_m^0}{k\Delta h_f}, \qquad (5)$$

where σ and σ_e are the side and end surface free energies per unit area, respectively, and Δh_f the heat of fusion per unit volume of a crystal. From the values of K and the parameters in Table 1, the values of $\sigma\sigma_e$ are calculated as 7.04×10^{-4} J^2 m^{-4} for the trigonal form and 1.68×10^{-4} J^2 m^{-4} for the tetragonal form. From the values of σ_e determined above, we obtain the values of σ to be 17.1×10^{-3} J m^{-2} for the trigonal form and 3.85×10^{-3} J m^{-2} for the tetragonal form.

4. Discussion

The value σ of the trigonal form we obtained above is 4.5 times as large as that of the tetragonal form. In this section, we first compare the values of σ of both forms with σ^{Hoff} estimated according to equation (1) and then discuss the mechanism that causes the difference between the values of σ of both forms.

Using the parameters listed in Table 1 and the characteristic ratio $C_\infty = 18.0$ of it-PB1 reported in the literature (Kurata & Tsunashima, 1999), σ^{Hoff} of the trigonal form is estimated as 2.38×10^{-3} J m^{-2} at 358.2 K from equation (1). This estimation is about one seventh the value of σ of the trigonal form obtained above from experiments and equation (1) does not hold. On the other hand, σ^{Hoff} of the tetragonal form at 358.2 K is estimated as 3.19×10^{-3} J m^{-2}, which is roughly in agreement with the experimentally obtained value of $\sigma = 3.85 \times 10^{-3}$ J m^{-2}. It is of much interest that equation (1) does not hold for trigonal crystals while it holds roughly for tetragonal crystals growing in the same environment.

Experimentally determined σ can have the error of -50% depending on the regimes assumed (Hoffman & Miller, 1997). If we assume regime III, i.e. rough surface growth mode, K is expressed as $4b\sigma\sigma_e T_m^0/k\Delta h_f$; σ is obtained as 8.55×10^{-3} J m^{-2}, which is half the value derived assuming regime II. However, this value is still 3.5 times larger than σ^{Hoff}. This excessively large σ value can not be explained.

The discrepancy between the values of σ and σ^{Hoff} for the trigonal form can be attributed to the loss of conformational entropy of the it-PB1 side chains; when an it-PB1 chain forms a nucleating stem of the trigonal form, it is assumed that the chain needs not only to become 'segmentalized and aligned', but also to have its side chains 'fixed' in the crystallographically correct conformation. The restricted conformation of the side chains generates an excessive amount of free

Figure 2
SAXS profiles for trigonal and tetragonal samples crystallized at 313.2, 343.2, 353.2, 363.2 and 373.2 K. The profiles have been shifted vertically for clarity.
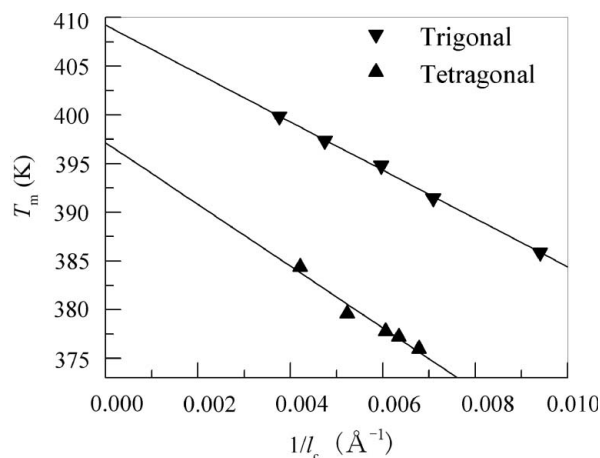
Figure 3
The dependence of the melting temperature T_m on the reciprocal lamellar crystal thickness l_c for trigonal and tetragonal crystals.

energy barrier due to the loss of conformational entropy of the side chains; this can account for the much larger value of lateral surface free energy σ than the value of σ^{Hoff} estimated from equation (1). If we assume that the ethyl side groups in the segmentalized-aligned it-PB1 chains should adopt the conformation which is the same as that inside the trigonal crystal phase, the loss of conformational entropy of a side chain in a monomer is roughly estimated as $k\ln 3$, since the ethyl side group of it-PB1 is an articulated side chain and the three rotational isometric states can clearly be distinguished. The increase of free energy barrier of nucleation per monomer due to the loss of conformational entropy of a side chain, Δf_{side}, is written as

$$\Delta f_{\text{side}} \simeq \left(1 - \frac{1}{C_{\infty}}\right)kT\ln 3, \qquad (6)$$

where the term $(-1/C_{\infty})$ in the first factor of the right hand side is added to subtract the free energy barrier already counted in equation (1), because the full entropy of fusion of both the side chains and main chains multiplied by a factor $1/C_{\infty}$ is considered to be the free energy barrier of forming a nucleating stem in the derivation of equation (1). The value of Δf_{side} is thus calculated to be 5.13 × 10^{-21} J at 358.2 K. On the other hand, the observed excessive amount of free energy barrier of nucleation per monomer, $\Delta\varphi_{\text{ex}}$, is represented by

$$\Delta\varphi_{\text{ex}} = 2l_{\text{m}}b(\sigma - \sigma^{\text{Hoff}}), \qquad (7)$$

where l_{m} is the size of the monomer as projected along the c axis and is equal to 2.17 Å for the trigonal form. Equation (7) yields the value of $\Delta\varphi_{\text{ex}}$ to be 5.67 × 10^{-21} J for the trigonal form. This is roughly in agreement with the value of Δf_{side}. The agreement indicates that the difference between the values of σ and σ^{Hoff} can be attributed to the loss of entropy caused by the conformational restriction of the side groups. We hence obtain the expression of σ of the trigonal phase related to σ^{Hoff} and Δf_{side} as follows:

$$\sigma = \sigma^{\text{Hoff}} + \frac{\Delta f_{\text{side}}}{2l_{\text{m}}b}. \qquad (8)$$

For the tetragonal form, $\Delta\varphi_{\text{ex}}$ is calculated to be 1.86 × 10^{-22} J, which is much smaller than that of the trigonal form. This is interpreted as follows: when an it-PB1 chain forms a nucleating stem in the tetragonal phase, on the contrary, the loss of conformational entropy of the side chains is much less effective. Maring et al. (1995) showed that the it-PB1 chains in the tetragonal phase have mobile and disordered conformation, while those in the trigonal phase have ordered and well rigid conformation from NMR data. Moreover, Miyoshi et al.
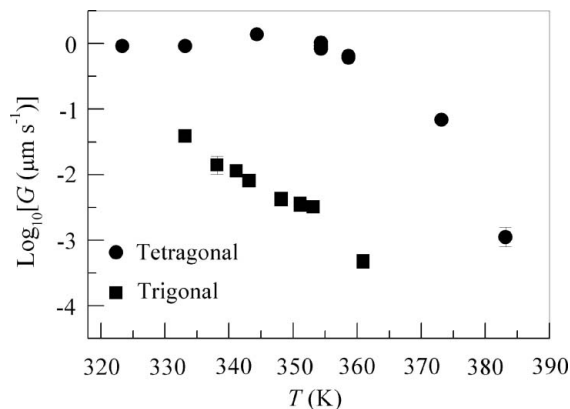
(2002) reported that the side chains of the tetragonal phase are disordered and highly mobile from NMR data. Due to the dynamic conformational disorder of the side chains of the tetragonal crystalline phase, side chains are considered to be imposed on much less conformational restriction; the loss of conformational entropy for the side chains to nucleate is much smaller and the 'segmentalized and aligned' state is the main part of nucleation barrier. This can account for the fact that equation (1) roughly holds for the tetragonal phase. [The trigonal phase is reported to have a statistically disordered structure (Natta et al., 1960; Tashiro et al., 1997). At one site of the lattice, upward and downward chains of the same helical handedness are statistically located at a weight of 50%. This means that the orientation of helices is statistically disordered, but this does not mean side chains are disordered within each helix. Side chains are considered to have ordered conformation within each helix, which helps make the loss of conformational entropy of side chains work as the barrier of nucleation.]

The trigonal phase of it-PB1 is the first experimentally demonstrated example of a polymer crystal whose lateral surface free energy σ clearly deviates from Hoffman's equation. In order to confirm our hypothesis, we need to investigate large numbers of polymers with different side chains. More precise and systematic investigations that deal with the size and symmetry of side chains are deemed necessary. A research is already under way on poly-methylpentene-1, which has more bulky isobutyl side chains.

5. Conclusions

We determined the lateral and end surface free energies of the trigonal and tetragonal crystals of it-PB1 grown in the melt from SAXS experiments, DSC measurements and in situ growth kinetics observations. Hoffman's equation of lateral surface free energy does not hold for the trigonal form, while it roughly holds for the tetragonal form. The disagreement of Hoffman's equation with the experiments for the trigonal form is considered to be caused by the conformational entropy of the ethyl side chains of it-PB1.

APPENDIX A
Derivation of Hoffman's equation

When a portion of a polymer chain constituted of m backbone C atoms becomes 'segmentalized and aligned' into sections of length $C_{\infty}l_{\text{b}}$, the fall in entropy as measured relative to the melt is expressed

Figure 4
Growth rate G vs crystallization temperature T for the trigonal and tetragonal forms. The errors are ±0.05 at most and can not be seen.
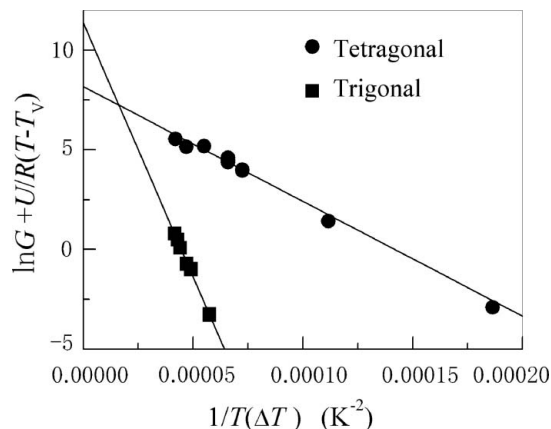
Figure 5
Plot of $\ln G + U/[R(T-T_{\text{V}})]$ vs $1/(T\Delta T)$.

as $-\Delta S_f/C_\infty$, where ΔS_f is the full entropy of fusion and is equal to $(\Delta h_f/T_m{}^0)abml_b$. The increase of free energy of this state is $T\Delta S_f/C_\infty$, which is interpreted as the barrier of nucleation and is equal to the work $2b\sigma ml_u$ of building the two lateral surfaces of a surface nucleating stem. Equating the work $2b\sigma ml_u$ with the barrier $T\Delta S_f/C_\infty$, equation (1) is obtained.

References

Andrews, R. J. & Grulke, E. A. (1999). *Polymer Handbook*, edited by J. Brandrup & E. H. Immergut, Vol. VI, pp. 206–207. New York: Wiley Interscience.

Danusso, F. & Gianotti, G. (1963). *Makromol. Chem.* **61**, 139–156.

Hoffman, J. D. (1992). *Polymer*, **33**, 2643–2644.

Hoffman, J. D., Davis, G. T. & Lauritzen, J. I. Jr (1976). *Treatise on Solid State Chemistry*, edited by N. B. Hannay, pp. 497–614. New York: Plenum.

Hoffman, J. D. & Miller, R. L. (1997). *Polymer*, **38**, 3151–3212.

Holland, V. F. & Miller, R. L. (1964). *J. Appl. Phys.* **35**, 3241–3248.

Kopp, S., Wittmann, J. C. & Lotz, B. (1994). *Polymer*, **35**, 916–924.

Kurata, M. & Tsunashima, Y. (1999). *Polymer Handbook*, edited by J. Brandrup & E. H. Immergut, Vol. VI, pp. 48–49. New York: Wiley Interscience.

Leute, U. & Dollhopf, W. (1983). *Colloid Polym. Sci.* **261**, 299–305.

Maring, D., Meurer, B. & Weill, G. J. (1995). *Polym. Sci. Part B Polym. Phys.* **33**, 1235–1247.

Miller, R. L. (1999). *Polymer Handbook*, edited by J. Brandrup & E. H. Immergut, Vol. VI, pp. 7–8. New York: Wiley Interscience.

Miyoshi, T., Hayashi, S., Imashiro, F. & Kaito, A. (2002). *Macromolecules*, **35**, 6060–6063.

Natta, G., Corradini, P. & Bassi, I. W. (1960). *Nuovo Cimento Suppl.* **15**, 52–67.

Powers, J., Hoffman, J. D., Weeks, J. J. & Quinn, F. A. Jr (1965). *J. Res. Natl Bur. Stand. Sect. A*, **69**, 335–345.

Spaepen, S. (1975). *Acta Metall.* **23**, 729–743.

Starkweather, H. W. Jr & Jones, G. A. (1986). *J. Polym. Sci. Part B Polym. Phys.* **24**, 1509–1514.

Tashiro, K., Asanaga, H., Ishino, K., Tazaki, R. & Kobayashi, M. (1997). *J. Polym. Sci. Part B Polym. Phys.* **35**, 1677–1700.

Tashiro, K., Saiani, A., Miyashita, S., Chatani, Y. & Tadokoro, H. (1998). *Polym. Prepr. Jpn*, **47**, 3869–3870.

Turnbull, D. & Spaepen, S. (1978). *J. Polym. Sci. Polym. Symp.* **63**, 237–243.

Turner-Jones, A. (1963). *J. Polym. Sci. Part B Polym. Lett.* **1**, 455.

Wilski, H. & Grewer, T. (1964). *J. Polym. Sci. Part C*, **6**, 33–40.

Yamashita, M., Hoshino, A. & Kato, M. (2007). *J. Polym. Sci. Part B Polym. Phys.* **45**, 684–697.

Yamashita, M., Miyaji, H., Izumi, K. & Hoshino, A. (2004). *Polym. J.* **36**, 226–237.

Zhang, B., Yang, D. & Yan, S. (2002). *J. Polym. Sci. Part B Polym. Phys.* **40**, 2641–2645.